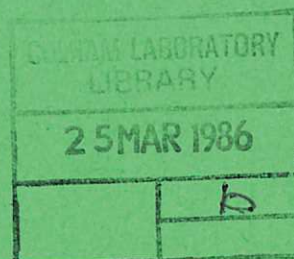


UKAEA

Preprint



STABILITY OF LOCALISED MHD MODES IN DIVERTOR TOKAMAKS A PICTURE OF THE H—MODE

C. M. BISHOP

CULHAM LABORATORY
Abingdon, Oxfordshire

1985

This document is intended for publication in a journal or at a conference and is made available on the understanding that extracts or references will not be published prior to publication of the original, without the consent of the authors.

Enquiries about copyright and reproduction should be addressed to the Librarian, UKAEA, Culham Laboratory, Abingdon, Oxon. OX14 3DB, England.

STABILITY OF LOCALISED MHD MODES
IN DIVERTOR TOKAMAKS
A PICTURE OF THE H-MODE

C.M. Bishop.

Culham Laboratory, Abingdon, Oxfordshire, OX14 3DB, UK
(Euratom/UKAEA Fusion Association)

Abstract

We examine the stability of a model divertor tokamak equilibrium to MHD ballooning and interchange modes. The combined effects of the magnetic separatrix and a finite edge current density can result in coalescence of the first and second stable regions. This leads to a picture of the H-mode in which the observed steep edge pressure gradients result from the modified ballooning stability properties.

(Submitted for publication in Nuclear Fusion)

November, 1985

1. Introduction.

Application of neutral injection heating to tokamak plasmas generally results in a degradation of energy confinement. However, tokamaks with poloidal divertors may exhibit an improved confinement regime, the H-mode, in which the confinement time is comparable to that observed with ohmic heating [1,2,3]. In such experiments the boundary of the plasma is defined by a magnetic separatrix. An outstanding feature of the H-mode is the occurrence just inside the separatrix of very steep gradients of density and temperature, and therefore of pressure. Since pressure gradients can be limited by the onset of ballooning and interchange modes it is of interest to examine how the stability properties of such modes are modified by the presence of the separatrix.

Recently [4] there has been interest in examining experimental pressure profiles (on ASDEX) for their stability to ideal ballooning modes. The theoretical criterion used, however, was the s - α model [5] which describes circular flux surfaces with constant poloidal field and which therefore neglects the presence of the separatrix and its effects on MHD stability. In a previous paper on ballooning stability in the vicinity of a separatrix [6] a model equilibrium was introduced to describe the plasma in a divertor tokamak. (This equilibrium represents a generalisation of the s - α model.) The present work generalises that of ref.[6] to allow for finite current density. We use a slightly modified equilibrium model and ballooning equation and for completeness we give a brief résumé of the equilibrium in section 2. We then examine the modified ballooning stability properties at zero current density. Stability of ballooning modes on the separatrix itself has been considered by Qu and Callan [7].

In section 3 we consider the stability of localised ideal interchange modes, and comment on the close connection between these and the ballooning modes. Appendix 1 deals with the stability of resistive interchange modes.

The effects on stability of a non-zero current density are investigated in section 4. This can result in a coalescence of first and second stable regions for flux surfaces sufficiently close to the

separatrix. The plasma in this region is then stable for any value of the pressure gradient. A possible explanation for this effect is described in section 5.

These results lead in section 6 to an interpretation of the H-mode in terms of ideal MHD stability properties. Quantitative predictions of the model are found to be in broad agreement with experimental results.

Conclusions are drawn in section 7.

2. Model Equilibrium and Ballooning Stability.

We begin with a brief review of the model divertor tokamak equilibrium, and the corresponding ballooning mode equation, introduced in reference [6]. Detailed construction of the equilibrium, and a derivation of the ballooning equation, have been given in reference [8].

Using a technique devised by Mercier and Luc [9] the Grad-Shafranov equation is solved locally by expansion in the neighbourhood of a single flux surface. The equilibrium is then determined once the shape of the surface, and the poloidal magnetic field on the surface, have been specified. This information is taken from the magnetic field structure surrounding a pair of long thin parallel wires carrying equal currents [10]. This linear vacuum system is used only to generate a single magnetic surface - the equilibrium itself is calculated in toroidal geometry at finite β . The shape of the magnetic surface is specified in polar coordinates (r, θ) by the implicit relation

$$k^2 = \frac{r^2}{r_o^2} [\sqrt{(1+k)} - 1]^2 \left\{ 4 + \frac{r^2}{r_o^2} [\sqrt{(1+k)} - 1]^2 - 4 \frac{r}{r_o} \cos(\theta - \gamma) [\sqrt{(1+k)} - 1] \right\}$$

$$r(\theta) = r_o g(\theta) \tag{1}$$

where k is a parameter controlling the shape of the surface such that as $k \rightarrow 0$ the surface becomes a circle, and as $k \rightarrow 1$ the shape of the surface approaches that of a separatrix. Eq.(1) is normalised so that the value of r opposite the X-point is held fixed ($r = r_o$) independent of k .

Examples of surfaces with different values of k are shown in Fig 1. This diagram also defines the angle γ which controls the poloidal location of the X-point.

The corresponding poloidal magnetic field on the flux surface is given by

$$\left\{ \frac{B_p(\theta)}{B_{po}} \right\}^2 = \frac{1 + \frac{r^2}{r_o^2} [\sqrt{(1+k)} - 1]^2 - \frac{2r}{r_o} [\sqrt{(1+k)} - 1] \cos(\theta - \gamma)}{(1+k)} = [b(\theta)]^2 \quad (2)$$

in which the value of the poloidal field opposite the X-point is held fixed at $B_p = B_{po}$ independent of k .

Throughout this paper we consider a large aspect ratio tokamak. We therefore write the major radius $X(\theta)$ at a point on the flux surface in the form

$$X(\theta) = X_o + \delta X(\theta)$$

where X_o is defined in Fig.1. We then take the high- β tokamak ordering

$$\frac{\delta X}{X_o} \sim \frac{r_o}{X_o} \sim \frac{p}{B^2} \sim \frac{B_p}{B} \sim \epsilon$$

(where p is the plasma pressure and B is the total magnetic field) and keep only the leading order contributions in a small- ϵ expansion.

The ballooning equation in large aspect ratio corresponding to this equilibrium can be written

$$\frac{b}{h} \frac{d}{d\theta} \left\{ \left[\frac{1}{b^2} + p^2(\theta) \right] \frac{b}{h} \frac{dF}{d\theta} \right\} - \alpha \{ \sin u + \cos u P(\theta) \} F = 0 \quad (3)$$

Here we have written the poloidal arc length as $dl = h(\theta)d\theta$ with

$$h(\theta) = [g^2 + (g')^2]^{1/2}.$$

The function $P(\theta)$ is defined by

$$P(\theta) = b \int_{\theta_0}^{\theta} \frac{hd\theta}{b^3} \left\{ \alpha + \frac{2b}{f} - \alpha \delta X \right\}$$

and u is the angle between the local tangent to the flux surface and the X -direction. Also $f(\theta) = R(\theta)/r_0$ where $R(\theta)$ is the gaussian radius of curvature of the flux surface given by

$$R(\theta) = \frac{[r^2 + (r')^2]^{3/2}}{[r^2 + 2(r')^2 - r r'']}$$

Finally we have introduced the parameters

$$\sigma = \left(p' + \frac{II'}{X_0^2} \right) \frac{X_0 r_0}{B_{p0}} \quad (4)$$

$$\alpha = - \frac{2p' r_0^2}{B_{p0}} \quad (5)$$

where $I(\psi)$ is the toroidal field function ($\underline{B} = (I/X)\underline{e}_\phi + \nabla\psi \times \nabla\phi$), ϕ is the toroidal angle, and primes denote derivatives with respect to the poloidal flux ψ . Note that the pressure gradient parameter α defined here reduces to the s - α definition [5] when $k \rightarrow 0$. As a consequence of the ballooning transformation [11] the poloidal angle θ in eq.(3) lies on $[-\infty, \infty]$. Eq.(3) is solved with the boundary conditions $F(\pm\infty) = 0$, and can be regarded as an eigenvalue equation for α .

In section 4 we shall be interested in studying the dependence of the stability properties on the toroidal current density. Although σ is closely related to the current density its value depends on the (arbitrary) definition of X_0 ; that is if we transform

$$X_0 \rightarrow X_0 + C, \quad \delta X \rightarrow \delta X - C \quad (6)$$

where $C/X_0 = O(\epsilon)$ then σ is not invariant at leading order in ϵ . This follows from the partial cancellation of p' and II'/X_0^2 :

$$(p' + II'/x_o^2)/p' = 0(\epsilon)$$

Thus under (6) we have

$$p' + \frac{II'}{x_o^2} \rightarrow p' + \frac{II'}{x_o^2} - 2 \frac{C}{x_o} \frac{II'}{x_o^2}$$

and the extra term must be retained at leading order. Instead of using σ we proceed as follows. From Ohm's law we can write

$$\eta \underline{J} \cdot \underline{B} = - \underline{B} \cdot \underline{\nabla} \Phi + \underline{B} \cdot \underline{E}^A$$

where \underline{E}^A is the inductive contribution to the electric field, η is the resistivity and Φ is the electrostatic potential. We can annihilate $\underline{B} \cdot \underline{\nabla} \Phi$ by integration round the flux surface (since Φ must be single-valued):

$$\oint \frac{dl}{B_p} \underline{B} \cdot \underline{\nabla} \Phi = 0$$

Writing $\underline{E}^A = E^A \underline{e}_\phi$, where $E^A = V/2\pi X$ and V is the loop volts, and using $\underline{J} \cdot \underline{B} = J_\parallel B = -I'B^2 - Ip'$ we have

$$- \eta \oint \frac{dl}{B_p} (I'B^2 + Ip') = \oint \frac{dl}{B_p} \frac{B_\phi V}{2\pi X} \quad (7)$$

It is convenient at this point to introduce a number of surface-averaged quantities defined as follows

$$\begin{aligned} W &= \frac{1}{2\pi} \oint \frac{hd\theta}{b} \frac{\delta X}{r_o}, & A &= \frac{1}{2\pi} \oint \frac{hd\theta}{b^3} \\ D &= \frac{1}{2\pi} \oint \frac{hd\theta}{b}, & H &= \frac{1}{2\pi} \oint \frac{hd\theta}{f b^2} \frac{\delta X}{r_o} \\ G &= \frac{1}{2\pi} \oint \frac{hd\theta}{b^3} \frac{\delta X}{r_o}, & F &= \frac{1}{2\pi} \oint \frac{hd\theta}{f b^2} \\ T &= \frac{1}{2\pi} \oint \frac{hd\theta}{b^2} \sin u \end{aligned} \quad (8)$$

We now expand (7) in large aspect ratio taking account of the partial cancellation in $p' + II'/X_o^2$, and keeping the leading order contribution. We then obtain

$$\Lambda = \alpha \frac{W}{D} - \sigma \quad (9)$$

where Λ is defined by

$$\Lambda = \left(\frac{r_o v}{2\pi X_o B_{po} \eta} \right) \quad (10)$$

Note that eq.(9) is invariant under (6).

We are interested in solving the ballooning equation on flux surfaces near the edge of the plasma. Since these will be relatively cool and therefore resistive we begin by setting the toroidal current density parameter Λ to zero and using eq.(9) to eliminate σ in eq.(3). This treatment of the edge region avoids the dependence on the arbitrary quantity X_o which occurs if σ is set to zero as was done in ref.[6]. As a result the solutions of the ballooning equation as compared to those of ref.[6] are somewhat modified.

Fig 2 shows a plot of α against k for $\gamma = \pi/2$ corresponding to the (single null) divertor configurations in ASDEX and DOUBLET III. These show two stable regions separated by a region unstable to ballooning modes. Figs. 3 and 4 show the corresponding plots for $\gamma = 3\pi/4$ corresponding to the PDX configuration and $\gamma = \pi$ in which the X-point is on the inside of the torus. Note that the first stability boundary is essentially independent of γ (this continues to hold when $\gamma < \pi/2$), while the second boundary shows a strong dependence on γ , with the unstable region shrinking as the X-point is moved further round to the inside of the torus. We can define a global shear parameter s by [6]

$$s = \frac{X_o r_o B_{po}}{q} \frac{dq}{d\psi} \quad (11)$$

which reduces to the s - α definition when $k \rightarrow 0$. An expression for s is derived in [8] and can be written

$$s = \frac{\sigma A + 2F - \alpha G}{D} \quad (12)$$

In Fig. 5 we plot s against k for values of α corresponding to the first stability boundary of Fig. 3. (Again we eliminate σ in favour of Λ , and set $\Lambda = 0$). We see that $s \rightarrow \infty$ as $k \rightarrow 1$ even though α remains finite. This is in marked contrast to the s - α model in which large shear implies a large value of the marginally stable α .

Consideration of cases with $0 \leq \gamma < \pi/2$ must be postponed until we have studied the effects of interchange modes in the next section.

3. Stability of Ideal Interchange Modes

The criterion derived by Mercier [12] states that ideal interchange modes will be unstable if $D_M < 0$ where

$$D_M = \frac{1}{4} + \frac{p'}{(2\pi q')^2} \left\{ \left(\frac{\partial}{\partial \psi} \oint \frac{dl}{B_p} - p' \oint \frac{dl}{B_p^3} \right) \oint \frac{B^2 dl}{x^2 B_p^2} \right. \\ \left. + (I^2 p' \oint \frac{dl}{x^2 B_p^3} - (2\pi q') I) \oint \frac{dl}{x^2 B_p^3} \right\} \quad (13)$$

Here $q(\psi)$ is the safety factor, and q' is evaluated in ref. [8]. Expanding in large aspect ratio and keeping the leading order contribution we obtain

$$D_M = \frac{1}{4} - \frac{\alpha (2AH - 2FG - AT)}{(\sigma A + 2F - \alpha G)^2} \quad (14)$$

where the various flux-surface integrals are defined in (8).

The limit $k \rightarrow 0$ represents the large aspect ratio tokamak with $B_p(\theta) = \text{constant}$. This is the s - α model introduced in ref. [10]. To see its connection with the present study we eliminate σ in favour of the

global shear s given by eq. (12). Note that s is invariant under (6). Using (12) to eliminate σ in (14), the marginal stability condition $D_M = 0$ becomes

$$s^2 = \frac{4(2AH - AT - 2FG)}{D^2} \alpha \quad (15)$$

In the limit $k \rightarrow 0$ we obtain $s^2 = 0$ showing that interchange modes are irrelevant for the s - α model.

As we did for ballooning modes we eliminate σ in eq.(14) in favour of Λ defined by eq.(9). The criterion for marginal stability $D_M = 0$ can then be written

$$\begin{aligned} & (G - WA/D)^2 \left[\frac{\alpha}{2} \right]^2 \\ & - (4AH - 2AT - 2FG - 2WAF/D - \Lambda AG + \Lambda WA^2/D) \left[\frac{\alpha}{2} \right] \\ & + (F - \Lambda A/2)^2 = 0 \end{aligned} \quad (16)$$

By numerical evaluation of the various loop integrals in (16) we can solve for the marginally stable α in terms of the parameters γ , k and Λ .

For $\gamma < \pi/2$ (and $\Lambda \geq 0$) eq.(16) has two positive roots defining the boundaries of the first and second stable regions. As $\gamma \rightarrow \pi/2$ so $\alpha \rightarrow \infty$ and for $\gamma > \pi/2$ the roots for α are negative. Thus for normal tokamak pressure profiles the interchange mode will always be stable whenever $\gamma \geq \pi/2$. For this reason it was not necessary to consider interchange modes in plotting Figs.2, 3 and 4.

Again we begin by considering $\Lambda = 0$ and in Fig.6 we plot α vs. k for $\gamma = 0$, corresponding to the divertor configuration in JT60. This figure also shows the corresponding first ballooning stability boundary obtained by solving eq.(3) with $\Lambda = 0$.

In Fig.6 the ballooning boundary has only been plotted as far as the interchange mode threshold. Beyond this the numerical solution of the

ballooning equation is no longer meaningful, and the stability boundary is determined by the interchange mode. This follows from the relation between ballooning and interchange modes discussed in [11].

Asymptotically the solution to the ballooning equation, eq.(3), behaves like

$$F(\theta) \sim F_1 \theta^{\lambda_1} + F_2 \theta^{\lambda_2}$$

where the two values of λ are

$$\lambda_1 = -\frac{1}{2} - \sqrt{D_M}, \quad \lambda_2 = -\frac{1}{2} + \sqrt{D_M}$$

For $D_M > 0$ only the small solution is acceptable since the large solution (even though it tends to zero if $D_M < \frac{1}{4}$) leads to a divergent energy functional δW . Numerically we distinguish these two solutions by solving the ballooning equation on a finite interval $(-\theta_{\max} < \theta < \theta_{\max})$ and imposing the boundary condition $F(\pm \theta_{\max}) = 0$. This has the effect of setting

$$\frac{F_2}{F_1} = -\theta_{\max} (\lambda_1 - \lambda_2)$$

Then provided θ_{\max} is sufficiently large we have $F_2/F_1 \rightarrow 0$ and we pick out only the small solution. (In practice we ensure that θ_{\max} is large enough by checking that the eigenvalue is insensitive to the value of θ_{\max} .) However, as we approach the Mercier stability boundary $D_M = 0$ we have $(\lambda_1 - \lambda_2) \rightarrow 0$ and we need to use ever larger values of θ_{\max} to pick out the small solution, until we exceed some numerical limitation. In the interchange unstable region both solutions are oscillatory and the numerical method breaks down completely. Although eigenvalues can still be found they can be distinguished from genuine solutions by their sensitivity to the value of θ_{\max} .

4. Effects of Finite Current Density

In this section we investigate the effects of non-zero values of the current density parameter Λ . We begin by considering $\gamma = 3\pi/4$ with

$k = 0.95$. From the previous section it follows that we do not need to consider interchange modes since the X-point is on the inside of the torus. Therefore, in Fig.7, we plot α against Λ for the first and second marginally stable ballooning boundaries. We see that for $\Lambda > 0.7$ the first and second regions have coalesced and there is no longer an instability to ballooning modes. In Fig.8 we plot α vs. k for $\gamma = 3\pi/4$ and $\Lambda = 0.8$. We see that for surfaces sufficiently close to the separatrix ($k \gtrsim 0.9$) there is no ballooning unstable region and hence no ballooning limit to the pressure gradient.

For $\gamma < \pi/2$ we again have to consider interchange modes. In Fig.9 we plot α against Λ for $\gamma = 0$ and $k = 0.95$. Again we see that first and second stable regions coalesce. However, the first stability boundary now extends down to $\alpha = 0$. The reason for this is easily seen by differentiating eq.(16) with respect to Λ at fixed k and γ . There will be a minimum in α at $\Lambda = 2F/A$ and the minimum value will be $\alpha = 0$. Since the removal of the unstable region requires a minimum in α , a point where $\alpha = 0$ will necessarily be present. In Fig.10 we plot α against k for $\Lambda = 0.8$ and $\gamma = 0$. (The first ballooning boundary is also shown.) Again we see the coalescence of the stability boundaries and the existence of a point where the marginal α vanishes.

5. Interpretation of the Absence of Ballooning Instabilities

A simple explanation for the absence of ballooning instabilities on flux surfaces sufficiently close to the separatrix can be given following ideas introduced in ref.[13]. This is very similar to the mechanism which stabilises the ballooning mode in a strongly indented bean-shaped plasma [14]. We begin by considering the local shear S defined by

$$S = - \frac{\mathbf{B} \times \nabla\psi}{|\nabla\psi|^2} \cdot \nabla \times \left\{ \frac{\mathbf{B} \times \nabla\psi}{|\nabla\psi|^2} \right\} \quad (17)$$

Ballooning modes tend to be localised along the field line in regions where the local shear is small or zero. In equilibrium an increased pressure gradient is balanced by a strengthening of the poloidal field on the outside of the torus, and this decreases the local shear and can reverse its sign. Further increase of pressure gradient causes the points

of zero local shear to move round the surface away from the region of destabilising curvature. The ballooning instability is usually encountered well before these points reach the good curvature region on the inside of the torus. However, if the equilibrium can be modified (in this case by the introduction of non-zero Λ) in such a way that the zeros of local shear always lie in the good curvature region then, as was shown in [13], the ballooning mode will always be stable. This provides a simple interpretation for the results of the previous section and leads to a rough estimate for the boundary of the ballooning unstable region.

Expanding (17) in large aspect ratio we obtain

$$S = \frac{N}{b^2(\theta)} \left\{ \alpha \frac{W}{D} - \alpha \frac{\delta X}{r_o} - \Lambda + \frac{2b(\theta)}{f(\theta)} \right\} \quad (18)$$

where $N = I/(X_o^3 r_o B_{po})$. The normalised surface-average of (18) gives the global shear, eq.(12). We also need to find the angle θ_K at which the normal curvature changes sign. This occurs when

$$K \propto \frac{1}{B^2} \frac{\partial}{\partial \psi} (p + \frac{1}{2} B^2) = 0$$

which in large aspect ratio reduces to $\partial X/\partial \psi = 0$. From [8] this is equivalent to $\sin(\theta_K) = 0$. Again we consider $\gamma = 3\pi/4$ and $k = 0.95$. Since the flux surface is not up-down symmetric there will be two values of θ at which K vanishes, these being $\theta_K = 0.635\pi$ and $\theta_K = -0.535\pi$. In Fig. 11 we show the ballooning unstable region on an $\alpha - \Lambda$ diagram (this is Fig. 7 replotted on a smaller scale). Also shown are the lines along which $S = 0$ at $\theta = \theta_K$ obtained by evaluating (18). In the region to the right of these lines the zero of local shear always occurs in the favourable curvature region, and so any ballooning instabilities must be confined to the remainder of the $\alpha - \Lambda$ diagram. This is indeed seen to be the case and supports the interpretation given above for the coalescence of the first and second stable regions.

6. A Picture of the H-Mode

The results of section 4 lead us to suggest the following simple picture of L- and H-mode régimes in divertor tokamaks. In the L-mode the edge temperature, and hence the current density, is relatively low and the stability diagram has the form shown in Fig.3. The edge pressure gradient is then ballooning limited. If the edge temperature can be raised (e.g. by the passage of a heat pulse from a sawtooth instability) then the corresponding increased current density can lead to a stability diagram like Fig.7. The edge pressure gradient can now become very steep. This corresponds to an increased temperature just inside the separatrix. The resulting increased current density maintains the form of the stability diagram, and leads to the bistable nature of the L-H transition. Further into the plasma the pressure gradient is again ballooning limited.

Using a value of $\Lambda = 0.7$ from Fig.6, together with the definition of Λ , eq.(10), and the Spitzer resistivity formula, we obtain $T_{\text{edge}} \approx 350\text{eV}$ in broad agreement with observed values. Also, using data from PDX published in ref.[3] Fig.6, we can compare the calculated stability diagrams with experimental values of α . For the L-mode we obtain $\alpha \approx 0.36$ which fits well with the first stability boundary of Fig.3. Similarly for the H-mode we obtain $\alpha \approx 3.6$ for the very steep profiles close to the separatrix. Comparison with Fig.7 shows that this value lies well into the second region of stability which is accessible because of the absence of the ballooning unstable region near the plasma edge. Further in from the separatrix the experimental H-mode profiles are less steep and give $\alpha \approx 0.52$ which can again be compared with Fig.7 and which is consistent with the end of the ballooning unstable zone at $k \approx 0.9$.

With the X-point on the outside of the torus we have seen that whenever the first and second stable regions coalesce there will be a flux surface on which $\alpha = 0$. This may have a bearing on the prospects for achieving H-mode operation in JT60, and could adversely affect the pressure profiles which might be obtained.

7. Conclusions

We have investigated the stability of a model divertor tokamak equilibrium to ideal ballooning modes and to ideal and resistive interchange modes. This work may also be of interest in connection with conventional tokamaks when a magnetic separatrix is introduced into the vacuum vessel such as has been proposed for JET [15]. Comparison of the stability diagrams for various values of γ (the poloidal location of the X-point) supports the conclusion, reached in ref. [6], that the stability properties get progressively better as the X-point is moved round to the inside of the torus. Inclusion of finite current density shows the possibility of achieving complete stability to ballooning and interchange modes for surfaces sufficiently close to the separatrix. This leads to a picture of the H-mode in which the absence of ballooning instability permits the very large edge pressure gradient.

I would like to thank J.W. Connor, R.J. Hastie and J.B. Taylor for many valuable discussions and comments throughout the course of this work. I would also like to thank P. Kirby for the use of his ballooning code in solving the various stability equations.

Appendix 1: Resistive Interchange Modes

The effect on interchange modes of allowing finite resistivity, and consequent field line reconnection, is to modify the Mercier criterion (11) to read [16]

$$D_R < 0$$

where

$$D_R = D_M - \left[\frac{1}{2} - H \right]^2$$

and

$$H = \frac{I_p'}{(2\pi q')} \oint \frac{B^2 dl}{X B_p^3} - \left\{ \frac{\oint \frac{dl}{B_p^3} \frac{1}{X}}{\oint \frac{B^2 dl}{X^2 B_p^3}} - \frac{\oint \frac{dl}{B_p}}{\oint \frac{B^2 dl}{B_p}} \right\} \quad (A1)$$

Again we expand in powers of the inverse aspect ratio and keep the leading order contribution. This yields

$$H = - \frac{\alpha (G - WA/D)}{(\sigma A + 2F - \alpha G)} \quad (A2)$$

where the various loop integrals are defined by (8). (At this order there are no cancellations between H and D_M to consider.) Using (12) for D_M we have

$$D_R = \frac{\alpha A \{T - 2H + 2WF/D + \Lambda G - \Lambda WA/D\}}{(\sigma A + 2F - \alpha G)^2} \quad (A3)$$

where again we have to eliminate σ in favour of Λ using eq.(9). Note

that (for $\alpha > 0$) the sign of D_R is independent of the value of α and depends only on γ , k and Λ . By inspection of eq.(19) we see that for $\Lambda = 0$ we have $D_R < 0$ if $\gamma < \pi/2$ and $D_R > 0$ if $\gamma > \pi/2$, so that the resistive interchange mode will be unstable if the X-point is located on the outside of the torus. For non-zero Λ the sign of D_R can be changed, and the mode stabilised.

References.

- [1] WAGNER, F., BECKER, G., BEHRINGER, K., CAMPBELL, D., EBERHAGEN, A., et. al., Phys. Rev. Lett. 49 (1982) 1408.
- [2] OHYABU, N., STAMBAUGH, R.D., DeBOO, J.C., EJIMA, S., PETRIE, T.W., et.al., in Plasma Science (Proc. IEEE Int. Conf. San Diego, CA, (1983) IEEE, New York (1983) 52.
NAGAMI, M., KASAI, M., AIKAWA, H., KITSUNEZAKI, A., KABAYASHI, T., et. al., in Controlled Fusion and Plasma Physics (Proc. 11th Europ. Conf. Aachen, 1983) Part I, ECA, Linnich (1983) 115.
- [3] KAY, S.M., BELL, M.G., BOL, K., BOYD, D., BRAU, K., et.al. J. Nucl. Mater. 121 (1984) 115.
- [4] KEILHACKER, M., GIERKE, G.V., MÜLLER, E.R., MURMANN, H., SOLDUER, F., et. al., Proc. 12th Europ. Conf. Budapest, (1985).
- [5] CONNOR, J.W., HASTIE, R.J., TAYLOR, J.B., Phys. Rev. Lett. 40 (1978) 396.
- [6] BISHOP, C.M., KIRBY, P., CONNOR, J.W., HASTIE, R.J., TAYLOR, J.B., Nucl. Fusion 24 No.12 (1984) 1579.
- [7] QU, W.X., CALLAN, J.D., Ballooning Instabilities on a Magnetic Separatrix, University of Wisconsin Report UWFD - 587 (1984).
- [8] BISHOP, C.M., Construction of Local Axisymmetric MHD equilibria, UKAEA, Culham Lab., Abingdon, Rep. CLM - R249 (1985)
- [9] MERCIER, C., LUC, N., MHD Approach to Confinement in Toroidal Systems, Commission of the European Communities, Brussels, Rep. EUR - 5127e (1974) 140.

- [10] HOBBS, G.D., TAYLOR, J.B., The Properties of Linear Filamentary Multipole Magnetic Fields, UKAEA, Culham Lab., Abingdon, Rep. CLM - R95 (1968).
- [11] CONNOR, J.W., HASTIE, R.J., TAYLOR, J.B., Proc. R. Soc. (London), Ser. A 365 (1979) 1.
- [12] MERCIER, C., Nucl. Fusion, 1 (1960) 47.
- [13] GREENE, J.M., CHANCE, M.S., Nucl. Fusion, 21 (1981) 453.
- [14] CHANCE, M.S., JARDIN, S.C., STIX, T.H., Phys. Rev. Lett. 51, No.21 (1983) 1963.
- [15] TANGA, A., CAMPBELL, D.J., DEUVE, B., GIBSON, A., GOTTARDI, N., et. al., in Controlled Fusion and Plasma Physics (Proc. 12th Europ. Conf. Budapest 1985) Part I (1985) 70.
- [16] GLASSER, A.H., GREENE, J.M., JOHNSON, J.L., Phys. Fluids 18 (1975) 875.

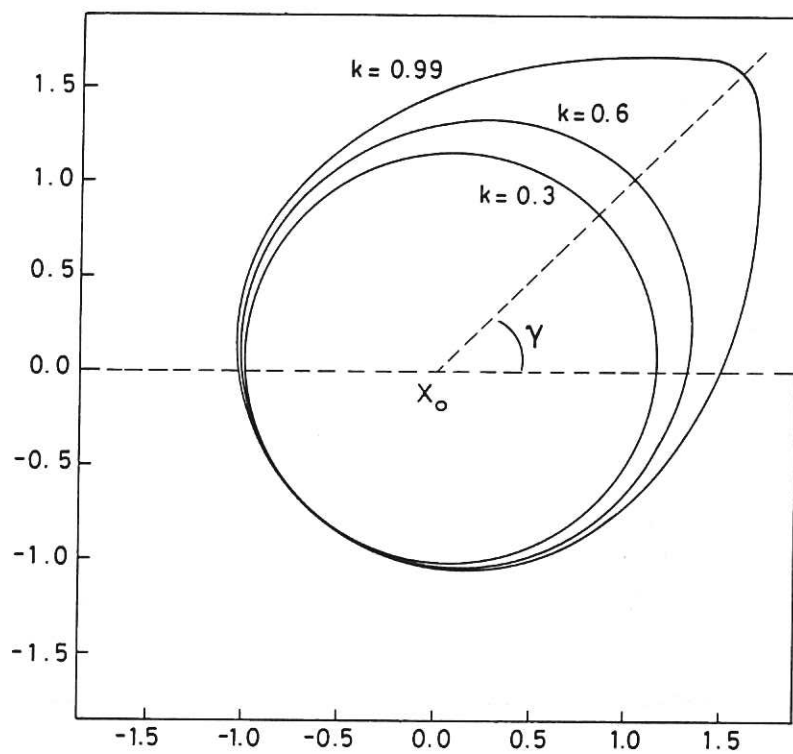


Fig.1 Plot of the magnetic surfaces for various values of k .

CLM-P764

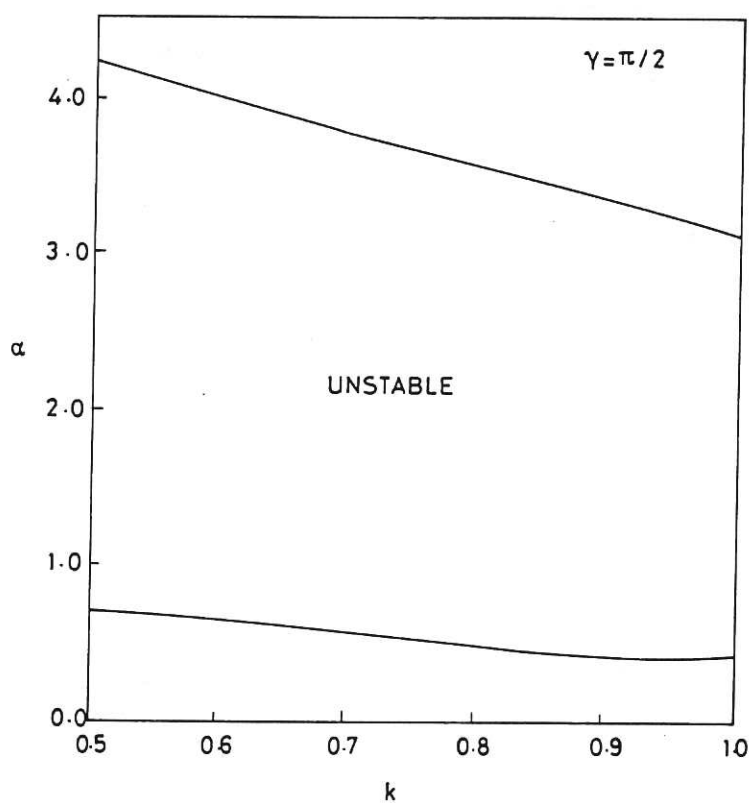


Fig.2 Marginally stable α as a function of k for $\gamma = \pi/2$.

CLM-P764

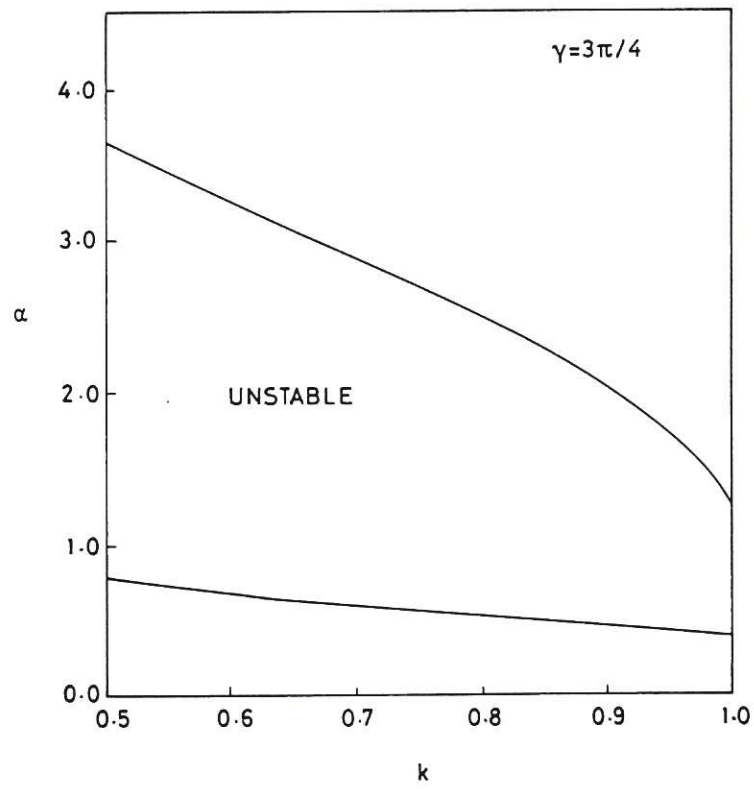


Fig.3 Marginally stable α as a function of k for $\gamma = 3\pi/4$.

CLM-P764

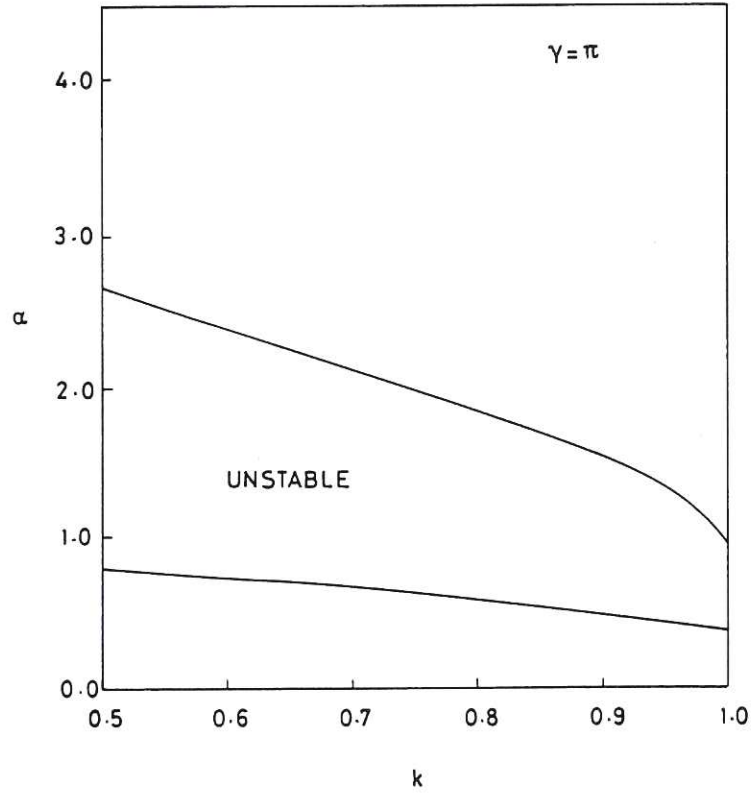


Fig.4 Marginally stable α as a function of k for $\gamma = \pi$.

CLM-P764

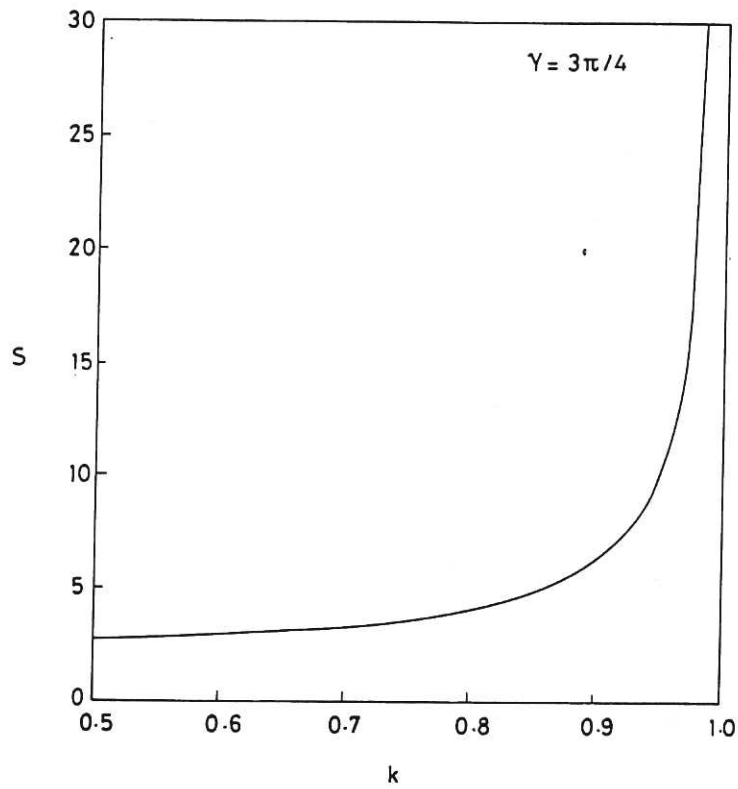


Fig.5 Global shear s as a function of k , along the first stability boundary of Fig.3.

CLM-P764

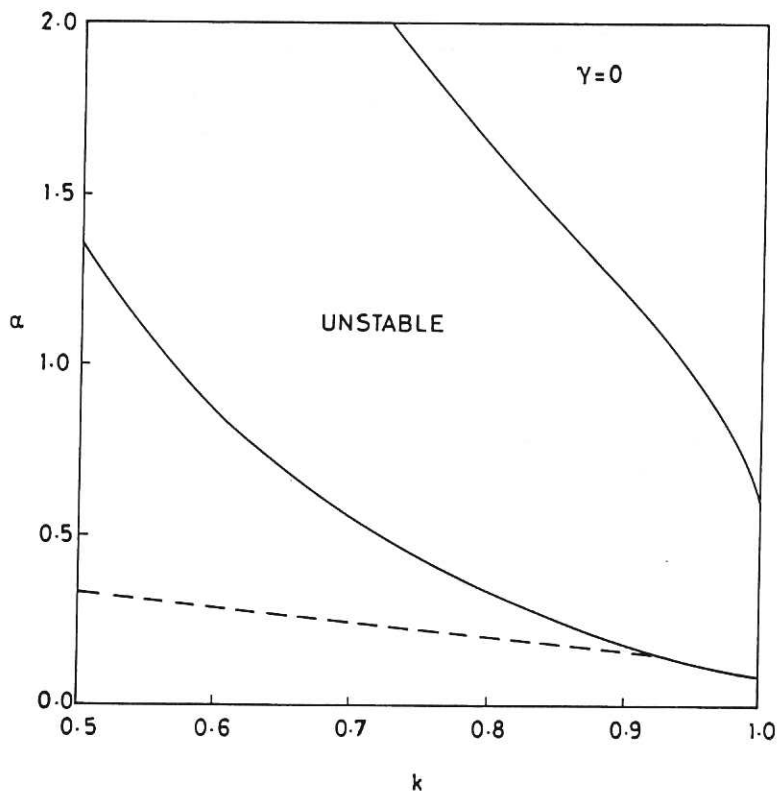


Fig.6 Marginally stable α for interchange modes as a function of k for $\gamma=0, \Lambda=0$. First ballooning boundary shown by broken line.

CLMP-764

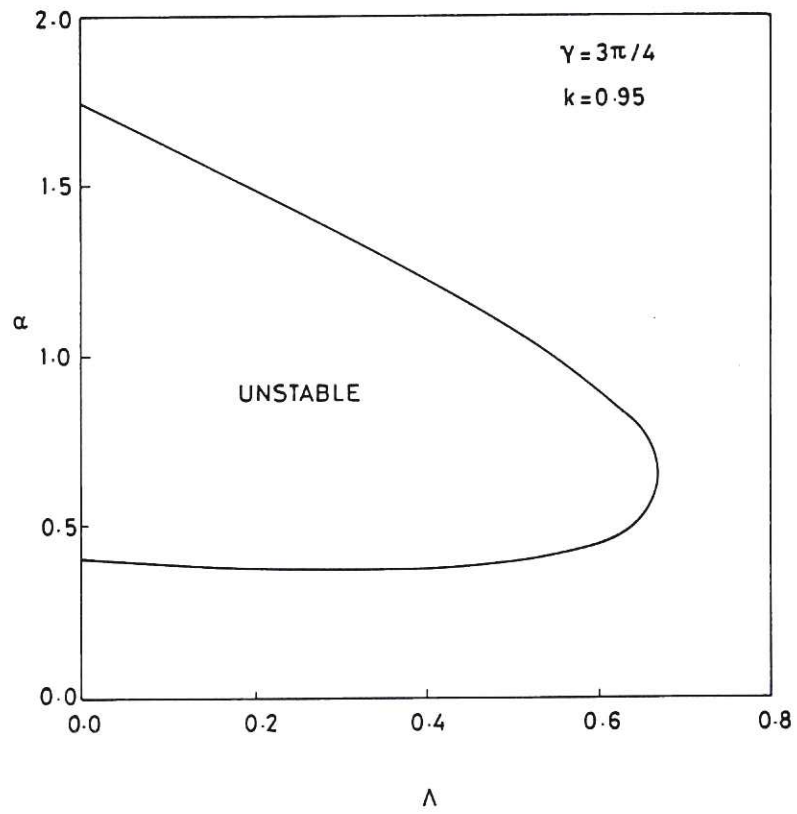


Fig.7 Marginally stable α as a function of Λ for $\gamma=3\pi/4$, $k=0.95$ showing coalescence of first and second stable regions.

CLM-P764

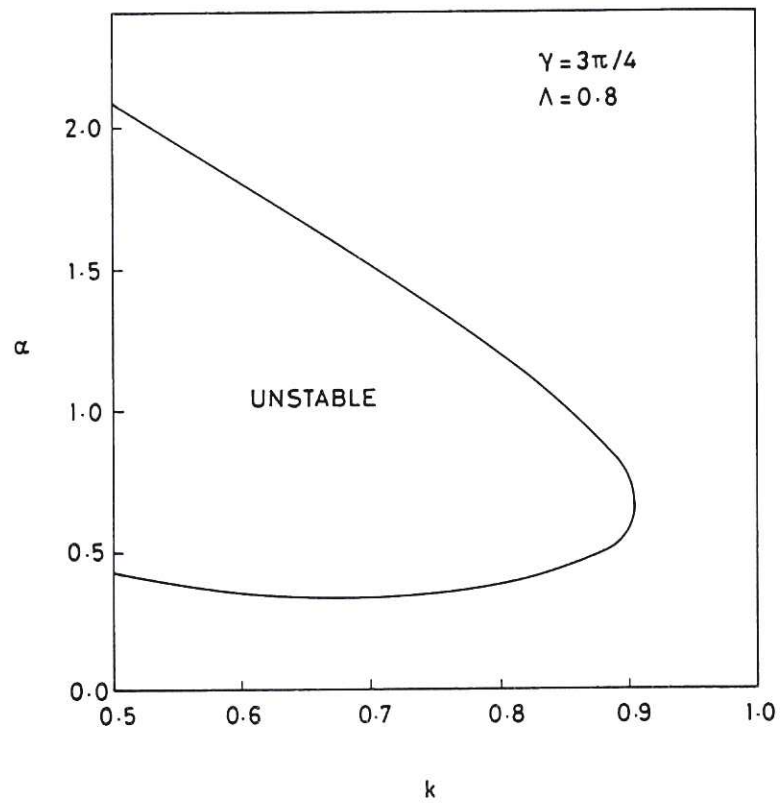


Fig.8 Marginally stable α as a function of k for $\gamma=3\pi/4$, $\Lambda=0.8$ showing the absence of the unstable region near the edge of the plasma.

CLM-P764

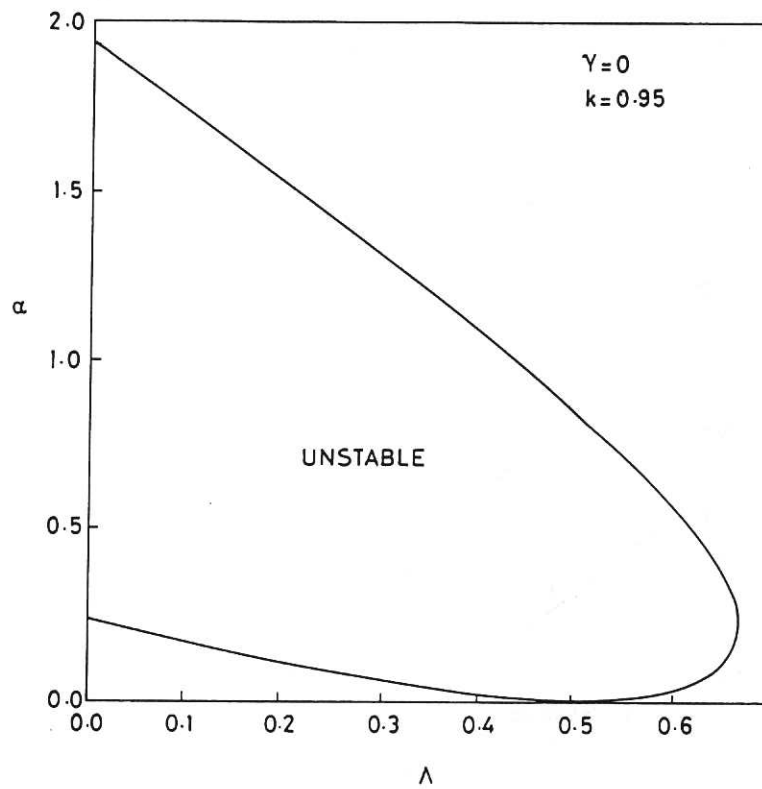


Fig. 9 Marginally stable α for interchange modes as a function of Λ for $\gamma=0$, $k=0.95$.

CLM-P764

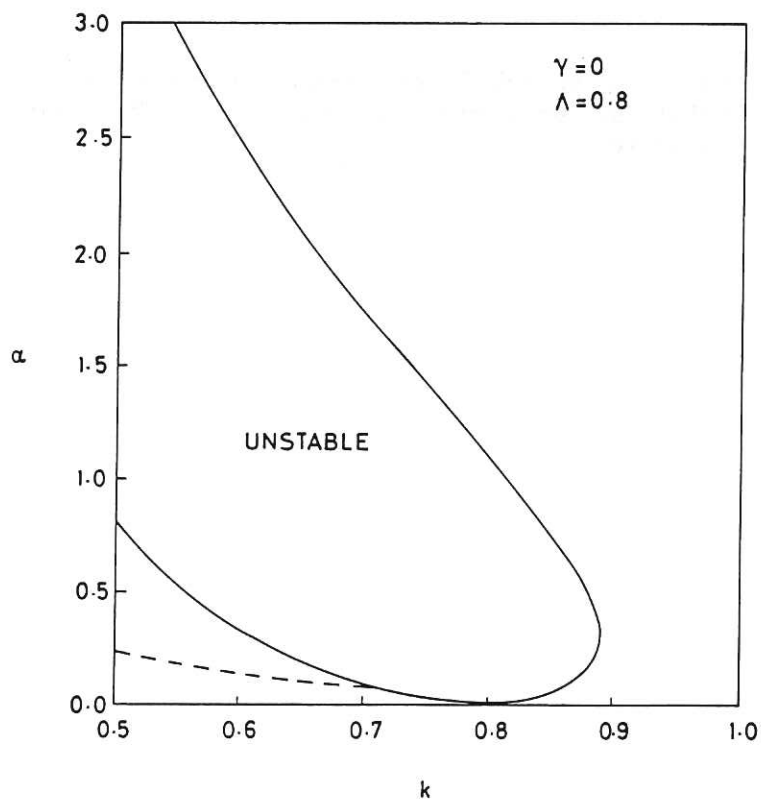


Fig. 10 Marginally stable α for interchange modes as a function of k for $\gamma=0$, $\Lambda=0.8$. First ballooning stability boundary shown by broken line.

CLM-P764

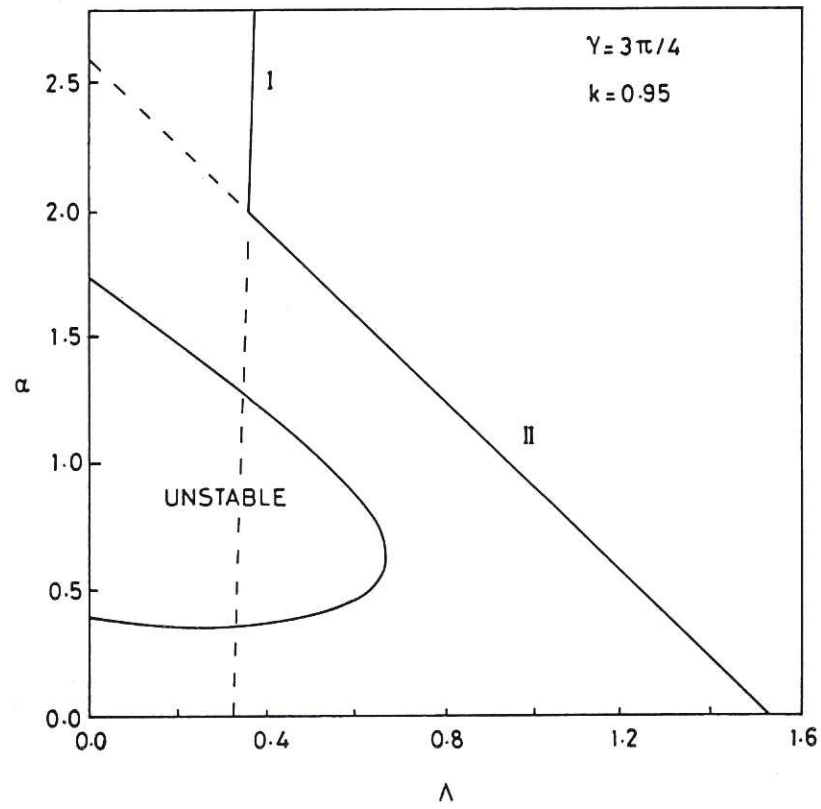


Fig. 11 This shows Fig. 7 replotted on a smaller scale together with the lines along which $S=0$ at $\theta=\theta_k$. (I $\theta_k=0.635\pi$ and II $\theta_k=-0.535\pi$).

CLM-P764



